

# Manipulation of anisotropic reflections based on optical models using multiple projectors

Shogo Ohsumi<sup>1</sup>, Toshiyuki Amano<sup>2</sup>

<sup>1,2</sup> *Wakayama University, 930, Sakaedani, Wakayama-shi, Wakayama, Japan*

## Abstract

This paper proposes a novel appearance-manipulation technique that parametrically manipulates the visible anisotropic reflection property with illumination projection from multiple projectors. This method obtains a reflectance matrix corresponding to the bidirectional reflectance distribution function (BRDF) from images captured using multiple cameras. The reflectance matrix was then fitted to the Ashikhmin BRDF model to estimate its parameters of the BRDF model. The reflectance matrix corresponding to the target BRDF was then calculated by manipulating the estimated parameters. The anisotropic reflection was manipulated based on the optical model by projecting images from multiple projectors that changed the texture represented by the reflectance matrix calculated in this manner.

## Keywords

Anisotropy, Light-field projection, BRDF.

## 1. Introduction

The angular light intensity distribution on the surface is formed by its properties (e.g., bidirectional reflectance distribution function (BRDF), bidirectional transmittance distribution function (BTDF)) and represents rich materiality, such as glossy metallic reflection, clear glass caustic, and beautiful structural color. Meanwhile, precisely designed light-field projection, instead of normal environmental illumination, has the potential to manipulate light angular distribution and alter our perception of materiality [1-4]. Such material appearance manipulation is a key challenge in spatial augmented reality (SAR), known as projection mapping. This paper proposes an anisotropic reflection property manipulation, which is an angular distribution manipulation of the reflected light ray on an anisotropic reflection surface using light field projection as a novel SAR technique.

## 2. Related work

### 2.1. Auto-stereoscopic display

Horizontally aligned projectors and a screen composed of lenticular lenses with a diffusing screen can achieve a projection-based autostereoscopic display [5,6]. Jones et al. [7] demonstrated a wide-viewing and high-angular-resolution autostereoscopic 3D display using 216 projectors. Naganu et al. [8] proposed an autostereoscopic projection display with 72 overlay images projected onto a vertically oriented lenticular screen with black back. Such front-projection auto-stereoscopic displays can be used to show complex materiality on an object using retroreflection paint on a 3D object [9]. However, they only displayed a BRDF and did not realize the alternation or manipulation of the BRDF that the object originally had.

### 2.2. VDDAM

Amano et al. [10] demonstrated view-direction dependent appearance manipulation (VDDAM), using multiple projector-camera feedback systems. Murakami et al. [11] proposed another method for VDDAM based on reflectance measurement among multiple projectors and cameras, which was equivalent to roughly sampled BRDF. Amano and Yoshioka [12] combined reflectance analysis with multiple projector-camera feedback and expanded the applicable reflection property to retroreflection and improved robustness against

<sup>1</sup>Corresponding author.

APMAR'22: The 14th Asia-Pacific Workshop on Mixed and Augmented Reality, Dec. 02-03, 2022, Yokohama, Japan  
EMAIL: s226042@wakayama-u.ac.jp (Shogo Ohsumi); amano@wakayama-u.ac.jp (Toshiyuki Amano)  
ORCID: 0000-0002-1393-8757 (Shogo Ohsumi); 0000-0003-4146-1375 (Toshiyuki Amano)



© 2022 Copyright for this paper by its authors. Use permitted under Creative Commons License Attribution 4.0 International (CC BY 4.0).

environmental lighting changes. However, the parameters for anisotropy are unknown for Amano et al. [10], whereas Murakami et al. [11] and Amano and Yoshioka [12] must consider in advance what type of anisotropy was used to create the target image.

In this paper, we propose a method to parameterize the VDDAM applying the Ashikhmin BRDF model to the previously acquired reflection characteristics. With this parameterization, we enhanced or reduced the anisotropy and then recreated the reflectance. Finally, we calculated the manipulation references for each viewing direction using the recreated reflectance.

### 2.3. Reflectance matrix

Murakami and Amano proposed a response model for multiple projectors and cameras that considers color [11]. The RGB values at a point A in the captured and projected images are defined as follows:

$$\hat{\mathbf{C}}_i = (c_i^r, c_i^g, c_i^b)^T, c_i^r \geq 0, c_i^g \geq 0, c_i^b \geq 0, \quad \text{where } i = 1, 2, \dots, u, \quad (1)$$

$$\hat{\mathbf{P}}_j = (p_j^r, p_j^g, p_j^b)^T, p_j^r \geq 0, p_j^g \geq 0, p_j^b \geq 0, \quad \text{where } j = 1, 2, \dots, v, \quad (2)$$

where  $u$  denotes the number of cameras, and  $v$  denotes the number of projectors. In this case, by expressing the reflection at an object surface as a matrix  $\hat{\mathbf{K}} \in \mathcal{R}^{3 \times 3}$ , it can be described as follows:

$$\hat{\mathbf{C}}_i = \hat{\mathbf{K}}_{ij} M_{ij} \hat{\mathbf{P}}_j, \quad (3)$$

where the matrix  $M_{ij}$  represents the color-mixing matrix [13] that calibrates the color. Furthermore, when multiple projectors or cameras are used, they are represented as follows:

$$\tilde{\mathbf{C}} = \tilde{\mathbf{K}} \tilde{\mathbf{M}} \tilde{\mathbf{P}}, \quad (4)$$

where

$$\tilde{\mathbf{C}} = (\hat{\mathbf{C}}_1^T, \hat{\mathbf{C}}_2^T, \dots, \hat{\mathbf{C}}_u^T)^T, \tilde{\mathbf{P}} = (\hat{\mathbf{P}}_1^T, \hat{\mathbf{P}}_2^T, \dots, \hat{\mathbf{P}}_v^T)^T, \quad (5)$$

$$\tilde{\mathbf{M}} = \begin{pmatrix} M_{11} & M_{12} & \dots & M_{1v} \\ M_{21} & M_{22} & \dots & M_{2v} \\ \vdots & \vdots & \ddots & \vdots \\ M_{u1} & M_{u2} & \dots & M_{uv} \end{pmatrix}, \tilde{\mathbf{K}} = \begin{pmatrix} \hat{\mathbf{K}}_{11} & \hat{\mathbf{K}}_{12} & \dots & \hat{\mathbf{K}}_{1v} \\ \hat{\mathbf{K}}_{21} & \hat{\mathbf{K}}_{22} & \dots & \hat{\mathbf{K}}_{2v} \\ \vdots & \vdots & \ddots & \vdots \\ \hat{\mathbf{K}}_{u1} & \hat{\mathbf{K}}_{u2} & \dots & \hat{\mathbf{K}}_{uv} \end{pmatrix}. \quad (6)$$

Hereafter, we regard the color spaces as calibrated, and we write  $\tilde{\mathbf{M}}\tilde{\mathbf{P}}$  as  $\tilde{\mathbf{P}}$  in the following sections.

### 2.4. Ashikhmin BRDF model[14]

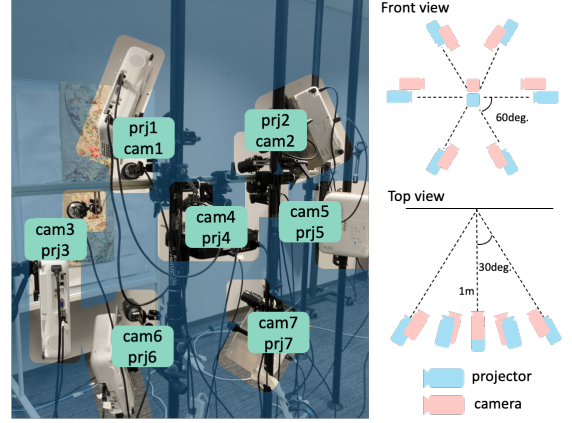


Figure 1: Experimental devices.

In this section, we introduce the Ashikhmin BRDF model to fit the reflectance matrix. The Ashikhmin BRDF model is described by the sum of the specular and diffuse components, with the specular component  $\rho_s$  defined as follows:

$$\rho_s(\mathbf{k}_1, \mathbf{k}_2) = \frac{\sqrt{(n_u+1)(n_v+1)}}{8\pi} \frac{(\mathbf{nh})^{\frac{(n_u(hu)^2+n_v(hv)^2)}{(1-hn)^2}}}{(\mathbf{hk}) \max((n\mathbf{k}_1), (n\mathbf{k}_2))} (R_s + (1-R_s)(1-(\mathbf{kh}))^5), \quad (7)$$

where  $\mathbf{k}_1$  and  $\mathbf{k}_2$  represent normalized vector to the light and viewer.  $\mathbf{h}$  represent normalized half-vector between  $\mathbf{k}_1$  and  $\mathbf{k}_2$ .  $\mathbf{n}$  represent surface normal to macroscopic surface.  $n_u$  and  $n_v$  represent two phong-like exponents that control the specular lobe shape. The larger the value of  $n_u$ , the higher the directivity of reflection in the  $\mathbf{u}$  direction. Similarly, the larger the value of  $n_v$ , the higher the directivity of reflection in the  $\mathbf{v}$  direction.

## 3. Proposed method

Our proposed method obtained a reflectance matrix representing the optical response between projectors and cameras corresponding to a roughly sampled BRDF on every single point on the object's surface with the experimental devices shown in Figure 1. Subsequently, we fitted the reflectance matrix with the Ashikhmin BRDF model and parameterized the reflectance relationship. Then, the parameters were manipulated to design a desired anisotropic reflection, yielding a recreated reflection matrix. Finally, the VDDAM based on the optical model achieved the desired appearance that the reflectance matrix represented by projecting images from multiple projectors.

### 3.1. Multiple projector-camera systems

In this paper, we employed 7 cameras (Ximea, MQ013CGE2, resolution:  $1280 \times 1024$ ) and 7 projectors (EPSON, EB-W05, resolution:  $1280 \times 800$ ) in order to achieve high quality perceptual BRDF manipulation with complex reflection characteristics. The cameras and projectors were placed in front of the target object and the other projectors are placed radially at  $15deg.$  intervals around the projector 4 (Figure 1). The cameras are placed close to each projector. This arrangement takes into account the measurement and manipulation of anisotropic reflections.

To obtain the reflectance matrix, first capture the red projection from one projector with all cameras. Similarly, the green and blue projection from one projector is captured by all cameras. This process is repeated with seven projectors. The reflectance is obtained by dividing the image thus acquired by the RGB of the projection image.

### 3.2. Manipulation Target Object

We used a drawing foil of Nishijin silk textile, which contains patterns of birds, flowers, clouds, and a mountain with rivers, as the manipulation target. Various threads, including gold thread and dyed thread, are used in this Nishijin silk textile, and differences in gloss can be seen, such as the gold thread being more reflective than the dyed thread. The weaving method also causes differences in reflectance characteristics. In the case of twill weave, the ratio of warp to weft threads on the surface is close, resulting in isotropic reflections. On the other hand, a satin weave has a higher ratio of warp threads than weft threads on the surface, resulting in anisotropic reflections. In this study, we regard the target object as a plane.

### 3.3. Parameter estimation

We employed the Levenberg-Marquardt method, a nonlinear optimization scheme, and obtained anisotropic reflection parameters by minimizing the error function as follows:

$$E(n_u^{st}, n_v^{st}, R_d^{st}, R_s^{st}) = \sum_{i=1}^I \sum_{j=1}^J (k_{ij}^{st} - \rho(\mathbf{k}_{1j}, \mathbf{k}_{2i}; n_u^{st}, n_v^{st}, R_d^{st}, R_s^{st}))^2, \quad (8)$$

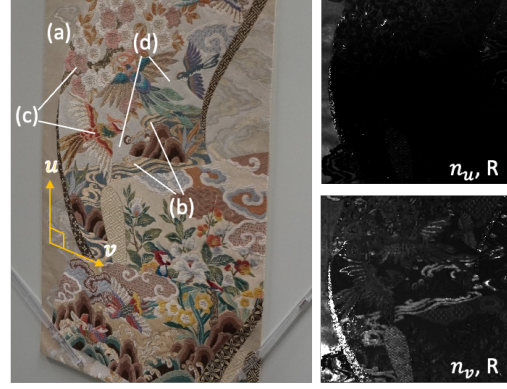


Figure 2: Operating object and an estimate of the  $n_u$  and  $n_v$  distributions.

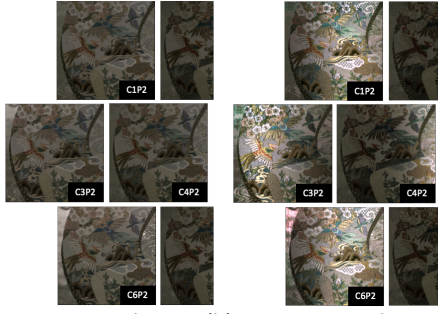
where  $s \in (r, g, b)$ ,  $t \in (r, g, b)$ , and  $k_{ij}^{st}$  represents the reflectance of the  $s$  color component of the  $t$  color projection of projector  $j$  captured by camera  $i$ .  $n_u^{st}, n_v^{st}$  represent anisotropic scattering for each direction, and  $\mathbf{u}, \mathbf{v}, R_d^{st}, R_s^{st}$  represent the intensities of the diffuse and specular components, respectively. Because the four parameters  $n_u, n_v, R_s$ , and  $R_d$  must be positive, we applied a non-negative condition to the Levenberg-Marquardt method. This allows us to obtain the four parameters of the Ashikhmin model for a single pixel from the reflectance matrix at a single pixel.

Figure 2 shows the estimated  $n_u$  and  $n_v$ . Because there is no significant difference the color channel, this figure shows only the R channel. Brightness expresses the value of each parameter, and the brighter area has a sharp specular reflection along each direction. A small difference between the  $n_u$  and  $n_v$  values indicates isotropy, whereas a large difference indicates anisotropy. Area (a) in the figure shows a twill weave using gold threads and has almost isotropic reflections. Area (b) is a satin weave that uses gold threads and exhibits strong anisotropy. Area (c) is a satin weave using dyed threads, and it has weak anisotropy. Area (d) is a twill weave using dyed threads and exhibits diffuse reflection.

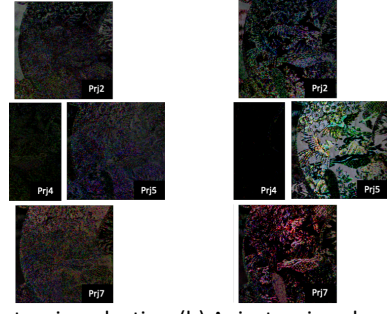
### 3.4. Anisotropy manipulation

Our anisotropic manipulation aims to enhance or reduce its reflection of the anisotropic reflection optically while maintaining the glossiness of the isotropic reflection. Based on this, we updated the parameters as follows:

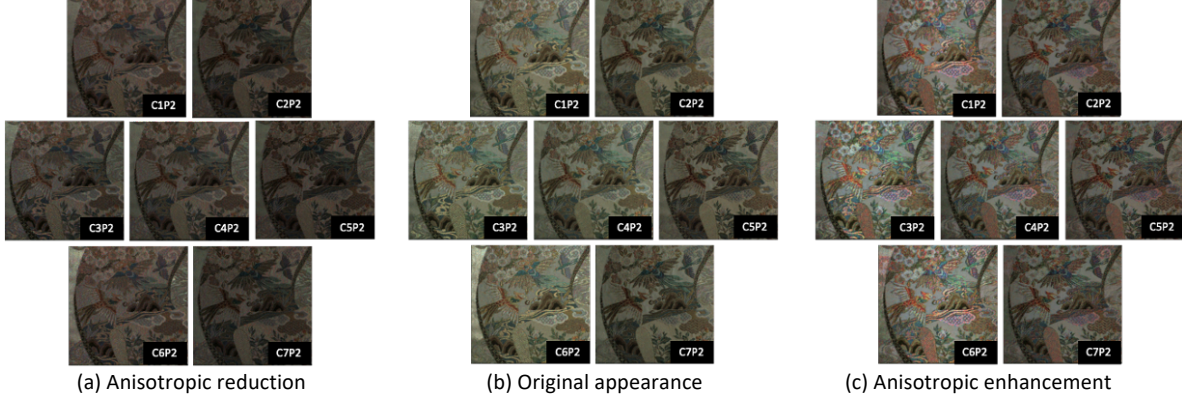
$$\begin{cases} n'_u = n_u + \alpha(n_u - n_v), & n'_v = n_v & (n_u \geq n_v) \\ n'_u = n_u, & n'_v = n_v + \alpha(n_v - n_u) & (n_u < n_v) \end{cases}. \quad (9)$$



(a) Anisotropic reduction (b) Anisotropic enhancement  
Figure 3: Target images.



(a) Anisotropic reduction (b) Anisotropic enhancement  
Figure 4: Projection images.



(a) Anisotropic reduction (b) Original appearance (c) Anisotropic enhancement  
Figure 5: Projection results.

If  $n_u$  was greater than  $n_v$ , the difference, which is an anisotropy, was added to  $n_u$  with a multiplication of the scaling factor  $\alpha$ . Otherwise, the difference was added to  $n_v$  as well. When  $\alpha > 1$ , the difference was expanded, and anisotropy was enhanced. On the contrary, the anisotropy was completely removed when  $\alpha = -1$ .

We applied this manipulation to the estimated parameters and obtained the desired target images for the entire manipulation area.

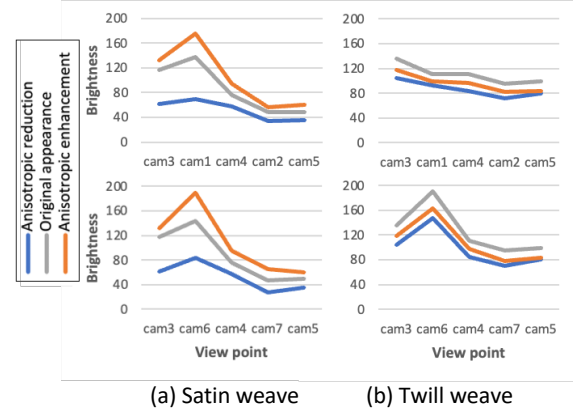
### 3.5. Calculation of projection image

From the reflectance matrix and the target images  $\tilde{\mathbf{C}}_t = (\tilde{\mathbf{C}}_{t1}^T, \tilde{\mathbf{C}}_{t2}^T, \dots, \tilde{\mathbf{C}}_{tu}^T)^T$ , we obtained the projection images  $\tilde{\mathbf{P}}_t = (\tilde{\mathbf{P}}_{t1}^T, \tilde{\mathbf{P}}_{t2}^T, \dots, \tilde{\mathbf{P}}_{tu}^T)^T$  for each projector. However, the projection images  $\tilde{\mathbf{P}}_t$  must be positive. Therefore, in this paper, a non-negative conditional optimization problem

$$\min_q \|\tilde{\mathbf{K}}\tilde{\mathbf{P}}_t - \tilde{\mathbf{C}}_t\|_2,$$

where  $p_{t1}^r \geq 0, p_{t1}^g \geq 0, p_{t1}^b \geq 0, \dots, p_{tv}^b \geq 0$ . (10)

used the Lawson-Hanson algorithm [15] to obtain the projection value of each projector at a certain point. This calculation was performed for all the points in the operating range to obtain the projection image for each projector.



(a) Satin weave (b) Twill weave  
Figure 6: Variation of brightness for each viewpoint.

## 4. Result

The target images were created by updating  $n_u$  and  $n_v$ , and by manipulating the value of  $\alpha$  in Eq. (9), the projection images were obtained using Eq. (10), and then projected.

Figures 3 and 4 shows examples of the target and projection images, respectively. In Figure 5, the projection results are arranged to correspond to each camera position. All of these images are shown in identical aspects by geometrical transformation to the common coordinate ( $cam\ 4$ ).

## 4.1. Anisotropic enhancement

Figure 3 shows the target images created using  $\alpha = 8$ . We solved the non-negative optimization problem described in Section 3.3 and obtained the projection images shown in Figure 4(b). The manipulation results from the projection are shown in Figure 5(c). It should be noted that a significant difference in glossiness between viewing directions along  $\mathbf{u}$  and  $\mathbf{v}$  was observed. Figure 6 shows the brightness change from *cam1* to *cam5* and *cam3* to *cam7* when the viewpoint is moved from left to right. Figure 6(a) shows the average brightness of the  $3 \times 3$  pixels in the area shown in Figure 2(b). When the viewpoint is moved horizontally in the range of *cam1* to *cam5* and *cam3* to *cam7*, the gloss change of the anisotropy enhanced image is sharper than that of the original appearance. These results confirmed the enhanced anisotropy.

Figure 6(b) shows the average brightness values of the  $3 \times 3$  pixels in the area shown in Figure 2(a). When the viewpoint is moved horizontally in the range of *cam1* to *cam5* and *cam3* to *cam7*, it can be confirmed that the anisotropic enhancement follows the brightness change of the original appearance, although the brightness of the anisotropic enhancement is reduced compared to the original appearance. This confirms that the isotropic reflection was maintained in the region of the gold thread twill weave.

## 4.2. Anisotropic reduction

Figure 3(a) shows the target images created with  $\alpha = -0.5$ . The projection images and manipulation results are shown in Figures 4(a) and 5(a), respectively. The overall images are darkened, however the central river area has lost its gloss. As shown in Figure 6(a), when the viewpoint is moved horizontally in the range of *cam1* to *cam5* and *cam3* to *cam7* in the region shown in Figure 2(b), the anisotropic reduction shows a smaller brightness change than the original appearance. From these results, we can confirm the reduction in anisotropy.

As shown in Figure 6(b), when the viewpoint is moved horizontally in the range of *cam1* to *cam5* and *cam3* to *cam7* in the region shown in Figure 2(a), the anisotropy reduction follows the brightness change of the original appearance, although the brightness of the anisotropy decreases compared to the original appearance. This confirms that isotropic reflection was maintained

even with anisotropic reduction in the region of the gold thread twill weave.

## 5. Conclusion

In this paper, we propose a method for estimating the parameters of the Ashikhmin model from the reflectance matrix. Furthermore, we propose a parameter manipulation method that can enhance and reduce anisotropy. Projection images were calculated using non-negative conditional optimization. The projection results showed that anisotropy could be enhanced and reduced in areas with anisotropic reflections. In areas with isotropic reflections, although the brightness was slightly reduced, the isotropic reflections were maintained.

## References

- [1] S. Shimazu et al., “3d high dynamic range display system”, ISMAR, pp.235–236, (2011).
- [2] T. Amano, H. Kato, “Appearance control using projection with model predictive control”, ICPR, pp.2832–2835, (2010).
- [3] T. Okazaki et al., “A projector-camera system for high-quality synthesis of virtual reflectance on real object surfaces”, IPSJ, pp.71-83, (2010).
- [4] A. J. Law et al., “Perceptually based appearance modification for compliant appearance editing”, CG Forum, 30(8), pp.2288-2300, (2011).
- [5] W. Matusik, H. Pfister, “3D TV: a scalable system for real-time acquisition, transmission, and autostereoscopic display of dynamic scenes”, SIGGRAPH, 23(3), pp.814-824, (2004).
- [6] R. Yang et al., “Toward the light field display: Autostereoscopic rendering via a cluster of projectors”, IEEE TVCG, 14(1), pp.84–96, (2008).
- [7] A. Jones et al., “An automultiscopic projector array for interactive digital humans” SIGGRAPH, (2015).
- [8] K. Nagano et al., “An autostereoscopic projector array optimized for 3D facial display”, SIGGRAPH, (2013).
- [9] T. Amano, K. Minami, “Structural color display on retroreflective objects”, ICAT - EGVE, pp. 37– 44, (2015).

- [10] T. Amano et al., "Viewpoint-Dependent Appearance-Manipulation with Multiple Projector-Camera Systems", ICAT-EGVE, pp.101-107, (2017).
- [11] K. Murakami, T. Amano, "Materiality Manipulation by Light-Field Projection from Reflectance Analysis", ICAT-EGVE, pp.99-105, (2018).
- [12] T. Amano, H. Yoshioka, "Viewing-Direction Dependent Appearance Manipulation Based on Light-Field Feedback", EuroVR, pp.192-205, (2020).
- [13] S. K. Nayar et al. "A projection system with radiometric compensation for screen imperfections", PROCAMS, (2003).
- [14] M. Ashikhmin, P. Shirley, "An anisotropic phong BRDF model", Journal of Graphics Tools, (2000).
- [15] C. L. Lawson, R. J. Hanson, "Solving least squares problems", (1974).